Wave-front propagation in a discrete model of excitable media

A. B. Feldman,* Y. B. Chernyak, and R. J. Cohen
Division of Health Sciences and Technology, Harvard University—Massachusetts Institute of Technology, Cambridge, Massachusetts 02139

(Received 4 December 1997)

We generalize our recent discrete cellular automata (CA) model of excitable media [Y. B. Chernyak, A. B. Feldman, and R. J. Cohen, Phys. Rev. E **55**, 3215 (1997)] to incorporate the effects of inhibitory processes on the propagation of the excitation wave front. In the common two variable reaction-diffusion (RD) models of excitable media, the inhibitory process is described by the v ''controller'' variable responsible for the restoration of the equilibrium state following excitation. In myocardial tissue, the inhibitory effects are mainly due to the inactivation of the fast sodium current. We represent inhibition using a physical model in which the ''source'' contribution of excited elements to the excitation of their neighbors decreases with time as a simple function with a single adjustable parameter (a rate constant). We sought specific solutions of the CA state transition equations and obtained (both analytically and numerically) the dependence of the wave-front speed c on the four model parameters and the wave-front curvature κ. By requiring that the major characteristics of $c(\kappa)$ in our CA model coincide with those obtained from solutions of a specific RD model, we find a unique set of CA parameter values for a given excitable medium. The basic structure of our CA solutions is remarkably similar to that found in typical RD systems (similar behavior is observed when the analogous model parameters are varied). Most notably, the ''turn-on'' of the inhibitory process is accompanied by the appearance of a solution branch of slow speed, unstable waves. Additionally, when κ is small, we obtain a family of ''eikonal'' relations $c(\kappa)$ that are suitable for the kinematic analysis of traveling waves in the CA medium. We compared the solutions of the CA equations to CA simulations for the case of plane waves and circular (target) waves and found excellent agreement. We then studied a spiral wave using the CA model adjusted to a specific RD system and found good correspondence between the shapes of the RD and CA spiral arms in the region away from the tip where kinematic theory applies. Our analysis suggests that only four physical parameters control the behavior of wave fronts in excitable media.
[S1063-651X(98)12706-X]

PACS number(s): 87.22.−q, 82.20.Wt, 82.40.Ck, 02.70.−c

I. INTRODUCTION

Traveling-wave patterns in excitable media have been studied extensively using continuous reaction-diffusion equation (RDE) models and discrete cellular automata (CA) models. The development of CA modeling approaches has been primarily motivated by their relative computational efficiency and ease of implementation on computers (though for some excitable media the discrete description may also be a more appropriate representation of the system [1]). CA simulations are an attractive alternative to solutions of coupled nonlinear RDEs, since these equations are often analytically intractable and usually too computationally burdensome to allow systematic numerical exploration of a system's parameter space (this is particularly true for models of myocardial tissue [2]). This aspect of CA modeling has caused the intuitive appeal of such models to receive much less attention. CA models in which the parameters have clear physical interpretations can also be useful vehicles for understanding complex behavior, such as the ''meandering'' of spiral waves and their interaction with spatial heterogeneities in the medium (both processes are believed to be important in cardiac fibrillation). An adequate description of the basic physical mechanisms controlling these processes has proved elusive via analysis of RDE solutions, though recently important progress has been made [3–6]. To be suitable for studying complex wave phenomena, the solutions of the discrete CA equations should be in good correspondence with those of the RDEs for a given physical system. In a recent article [7] we demonstrated that it was possible to quantitatively link the traveling-wave solutions of a general class of RDE models to those of a simple but appropriately constructed CA model in a physically self-consistent way. This analysis was valid for trigger waves, which arise in the limit when the recovery and other inhibitory processes are switched off. In this paper we establish the more general correspondence for the case of solitary wave fronts, which incorporate the effects of inhibitory processes on excitation. The demonstration of this correspondence represents an important step toward the development of quantitatively reliable CA models of continuous media.

Recent studies of complex wave patterns such as rotating spiral waves in CA models have demonstrated many qualitative and sometimes quantitative similarities between the CA solutions and the numerical solutions of specific RDEs [8–10]. This correspondence strongly suggests that in many cases these two representations of excitable media may be ''dynamically equivalent,''which means that the systems

*Author to whom correspondence should be addressed. Present address: Massachusetts Institute of Technology, 77 Massachusetts Avenue, Office E25-317, Cambridge, MA 02139. FAX: (617) 253-3019. Electronic address: afeldman@huhepu.harvard.edu

support the same wave patterns (e.g., plane waves, target waves, and spiral waves), exhibit similar behavior, and have similar responses when the analogous model parameters are varied. This implies the existence of a smooth mapping (not necessarily stationary) between the two systems. We previously found strong evidence of such equivalence for trigger waves using a simple three-parameter CA model of a two-dimensional, isotropic medium [7]. This analysis demonstrated the correspondence of the CA dependence of the wave speed c on the wave-front curvature κ with that of a general class of RDE models. Here we generalize the original CA model to represent solitary wave fronts and then examine in detail the changes in $c(\kappa)$ as the major CA parameters are varied. These changes are then compared to those found in simple RDE models under similar variations of the analogous parameters. We found remarkable similarities between the structure of the CA solutions and that typically found in the RDEs, including the appearance of a solution branch of slow-speed, unstable waves. This equivalent solution structure allows us to establish a quantitative mapping between the two representations of the system.

Our results are applicable to any physical process that reduces the magnitude of the excitatory current in the wave-front transition zone during the front's characteristic transition time. In myocardial tissue, the major inhibitory process is the inactivation (''turning off'') of the fast Na^+ current [11]. (The two-variable reaction-diffusion models considered in this article are only approximately applicable to myocardial tissue since the fast Na^+ current's contribution to the source term in the diffusion equation for the cell transmembrane potential is also activated (''turned on'') with nonzero time constant. The extent to which this contribution can be approximated as steady state, as well as the effect of this approximation on the values of important traveling wave parameters, requires further clarification [11]. See Ref. [12] for additional discussion of the limitations of two-variable RDE models of myocardium.) For clarity, however, our results are presented for a generic recovery process. The required modification of our original CA model involves the introduction of a monotonically decreasing function to describe the falloff of excitatory source current with time in the wave-front transition zone. The basic features of $c(\kappa)$ in the modified model do not appear to depend on the specific choice of this function, so for simplicity we performed the analysis using a simple linear falloff with a single adjustable parameter: a recovery rate constant γ. To adjust the CA model to a specific RDE system, we calculate γ and the three other CA parameter values by requiring that four major characteristics of $c(\kappa)$ coincide in both representations of the medium (for systems in which the RDEs are only approximately known, measured values may be preferred). These characteristics are the trigger plane-wave speed, the trigger wave critical curvature (the curvature at which $c=0$), the slope $dc(0)/d\kappa$ for trigger waves, and the speed of a plane solitary wave, which incorporates the correction to the trigger wave value due to the inhibitory process. This yields a set of four equations with a unique solution for the four CA parameter values. Our results strongly suggest that this procedure is sufficient for the correct physical representation of the excitation wave front. The matching of additional characteristics of the RDE solutions will be required to represent the deexcitation wave back and the partially refractory wave tail. These will be the subject of future work.

This paper is divided into seven sections. In Sec. II we discuss traveling solitary waves in RDE models [see Eqs. (1) and (2) below] and introduce the specific relationships needed for analysis of our CA model solutions. In Sec. III we generalize our CA model for trigger waves [7] by modifying the CA state transition equations to incorporate the temporal falloff of the source currents in the wave front region. The following two sections discuss the one-dimensional (1D) solitary front and 2D plane-wave-front solutions in the modified model (a proof of the instability of the slow speed solution branch for 1D CA solitary fronts is given in Appendix A). In Sec. VI we derive the specific equation determining the dependence of c on κ and analyze its solutions at large and small curvatures. We compute the ''critical curvature'' in the kinematic approximation, which is the maximal curvature for a stably propagating, continuous wave front, and also analyze the ''eikonal'' relation, which is the linear approximation to $c(\kappa)$ in the region of small κ. Finally, in Sec. VII we adjust the CA model parameters to represent a specific RDE system and compare the CA spiral wave solution to that obtained from the numerical solution of the RDEs.

II. WAVE FRONTS IN CONTINUOUS RDE MODELS

A minimum model of an excitable medium with a single diffusing quantity can be described by two variables u and v that obey a set of reaction-diffusion equations given in dimensionless form by

$$\frac{\partial u}{\partial t}=\nabla^2 u+f(u,v), \tag{1}$$

$$\frac{\partial v}{\partial t}=\varepsilon g(u,v), \tag{2}$$

where ∇^2 is the Laplacian operator in spatial coordinates (x,y,z), t is time, u represents the ''concentration'' of the diffusively propagating entity, and v is a recovery variable that controls the local recovery of excitability. The quantity ε is defined as $\varepsilon\equiv\tau_u/\tau_v$, where τ_u and τ_v are the characteristic time scales associated with the evolution of u and v, respectively. Usually $\varepsilon\ll 1$, which corresponds to fast excitation and slow recovery. The functions $f(u,v)$ and $g(u,v)$ in Eqs. (1) and (2) describe the nonlinear local kinetics of the system. For future reference, we shall call the function $f(u,v)$ the (reaction) source function and $-f(u,v)$ the (reaction) source current. To restore dimensions, the transformations $t\to t/\tau_u$ and $x\to x/\sqrt{D\tau_u}$ should be applied, where D is the diffusion coefficient of u.

The basic features of traveling waves in RDE systems can be seen via the analysis of a typical 1D solitary pulse solution. We shall consider the familiar, simple model with kinetic functions f and g given by [13,14]

$$f(u,v)=-\{i(u)+v\}, \tag{3}$$

$$g(u,v)=\zeta u-v, \tag{4}$$

where the function $i(u)$ is the piecewise linear current

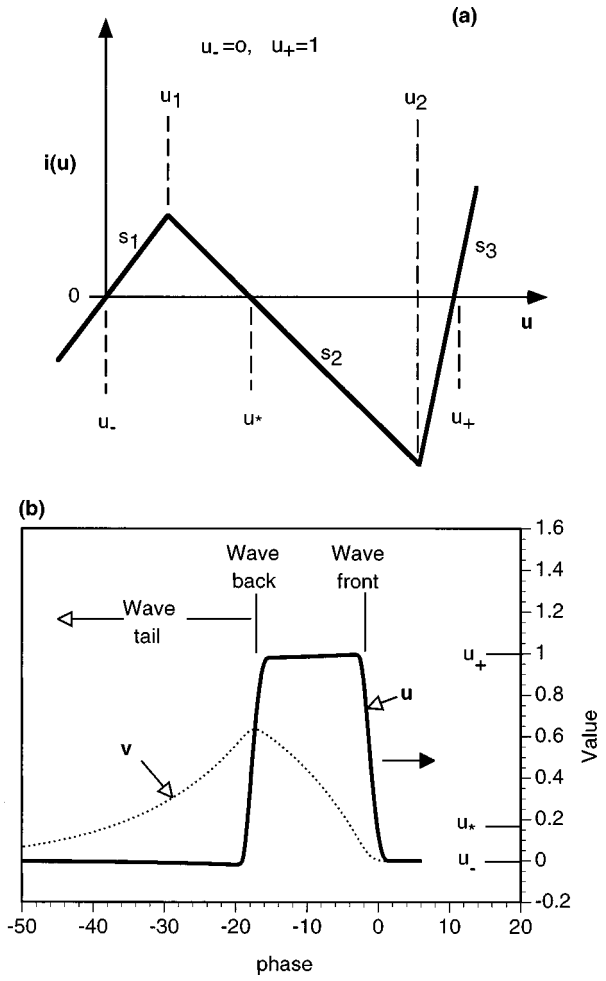

FIG. 1. (a) Piecewise linear current source $i(u)$ given by expression (5) and (b) 1D solitary pulse solution of Eqs. (1) and (2) for $f(u,v)$ and $g(u,v)$ given by Eqs. (3) and (4) with a specific $i(u)$. The parameter values used for the pulse were $s_1=30.0$, $s_2=0.9$, $s_3=30.0$, $\overline{u}=0.12$, $\zeta=1.0$, and $\varepsilon=0.06$ (see Ref. [13]). In (b), the behavior of u and v is shown as a function of the phase $\xi=x-c_0t$, where c_0 is the propagation speed. The direction of propagation is indicated by the arrow. The wave front, wave back, and wave tail are also indicated. All quantities shown are dimensionless.

$$i(u)=\begin{cases} s_1u & \text{when } u\leqslant u_1 \\ \overline{u}-s_2u & \text{when } u_1<u<u_2, \quad \overline{u}\equiv s_2u_* \\ s_3(u-1) & \text{when } u\geqslant u_2. \end{cases} \tag{5}$$

A plot of $i(u)$ is shown in Fig. 1(a). The constants s_1, s_2, and s_3 are all positive quantities. The current $i(u)$ has three consecutive roots u_-, u_*, and u_+, with the middle root u_* playing the role of an excitation threshold. The u coordinates of the beginning point and end point of the negative slope region are $u_1=\overline{u}/(s_1+s_2)$ and $u_2=(\overline{u}+s_3)/(s_2+s_3)$, respectively. A 1D solitary pulse solution of this system is shown in Fig. 1(b), which depicts the variation of u and v with the phase $\xi=x-c_0t$ for a pulse with constant speed c_0. The resting state (u_-, v_-) of the system is (0, 0). In the trigger wave limit ($\varepsilon=0$), the wave profile is described by the rise of u from its ''resting state'' value $u=u_-$ to its ''excited state'' value $u=u_+$. For ε small, the recovery variable v varies slowly during the rapid upstroke of u and is displaced from its resting value v_- by a small correction εv_1, where v_1 is a constant depending on the $\varepsilon=0$ solution [15]. On the plateau of the pulse, the spatial and temporal derivatives of u are small and u approximately follows the slow evolution of v adiabatically, so at each phase ξ, $u(\xi)$ is given by the solution of $f(u(\xi),v(\xi))=0$. When v approaches a specific maximum value, the deexcitation (or wave-back) transition takes place. Following this transition, the system slowly relaxes back to the equilibrium state (u_-,v_-). This relaxing region is called the wave tail. We shall focus our subsequent analysis on 1D and 2D *wave fronts* and consider propagation only in a *fully recovered* medium in its equilibrium state.

Figures 2(a) and 2(b) illustrate the deviations from the trigger wave limit in the wave-front transition region near $\xi=0$ for the 1D pulse. Figure 2(a) plots the u value versus the phase ξ of the wave, with zero phase defined to be the front crossing at $u=u_*$. The length scale L_0 of the wave-front transition region is a quantity of order D/c_0. The recovery effects due to nonzero ε result in corrections in a region extending approximately $-L_0<\xi<L_0$ that reduce the pulse speed relative to that of the trigger wave (the reduction is $\approx 5\%$ for the pulse in Fig. 2). The primary cause for this reduction is seen in Fig. 2(b), which plots the local values of the source current $-f(u,v)$ for the pulse in Fig. 2(a). The important feature of this plot is that when u sufficiently exceeds u_*, the magnitude of the pulse source current (bold curve) diminishes relatively to that of the trigger wave (dotted curve) and the deviation grows as ξ grows in magnitude until u approaches $u_+=1$. This effective reduction in amplitude of the excitatory source in Eq. (1) results in the reduced speed, since c_0 scales roughly as the square root of the source amplitude [16,17]. We note that in both the trigger wave and pulse cases, the source current $-f(u,v)$ changes sign at (and near, respectively) the point where $u=u_*$ and becomes ''excitatory,'' meaning that its contribution in Eq. (1) has the same sign as $\partial u/\partial t>0$. We now consider a snapshot of the front by setting $t=0$ in $\xi=x-c_0t$. At points on the front $u=u(x)$ with u values larger that that of the front's inflection point u_i $(u_*<u_i<u_2)$, the source current must overcompensate for the diffusion of u since $d^2u/dx^2<0$. The source currents in this region of the front may be thought of as the sources of the diffusive flux to regions below the inflection point where $d^2u/dx^2>0$ (sinks). The difference between the pulse and trigger wave source current values increases with the distance x_i-x, where x_i is the x coordinate of the inflection point. In terms of local time (setting $x=0$ in $\xi=x-c_0t$), this deviation can also be viewed as an increasing function of the (scaled) time elapsed since the crossing at $u=u_i$. Finally, we note that as u approaches u_+, the pulse source current again changes sign and assumes small positive (deexcitatory) values, while for the trigger wave it approaches zero asymptotically via negative (excitatory) values as $\xi\rightarrow-\infty$. The above features of the source currents in the front transition region form the physical basis for our CA model of inhibitory effects discussed in Sec. III.

The plane-solitary-wave speed c_0 in the medium [Eqs. (1)–(5)] depends on the specific value of the threshold u_*,

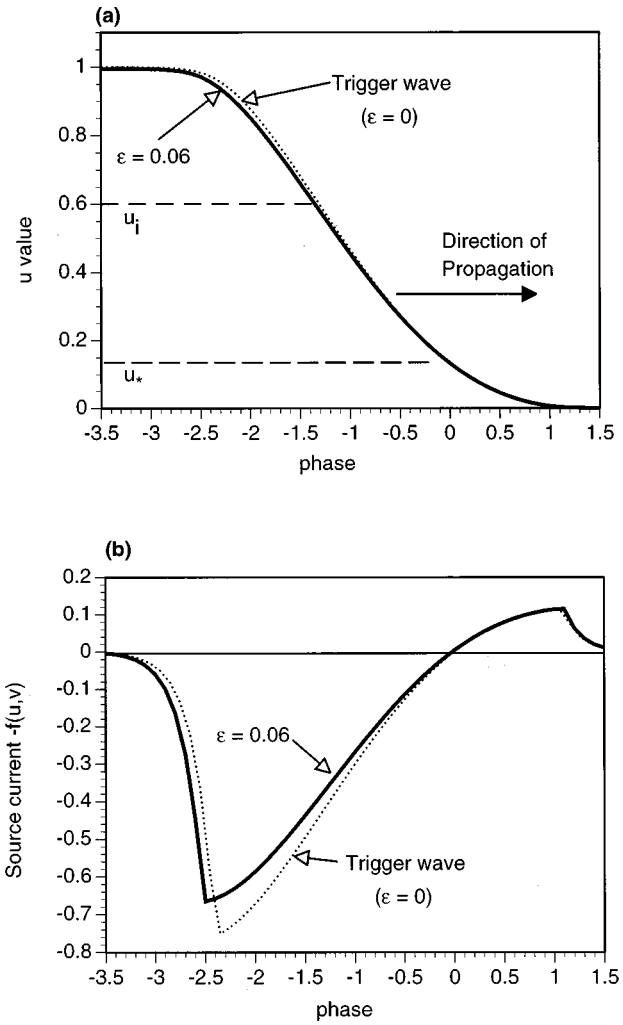

FIG. 2. The wave-front profiles $u(\xi)$ (a) and (b) the local source currents $-f(u,v)$ for the 1D solitary pulse in Fig. 1(b) and the trigger wave ($\varepsilon=0$) solution. The middle root u_* of $i(u)$ and the u value $u=u_i$ of the front's inflection point are indicated. The recovery process results in small corrections to u and $f(u,v)$ over the front transition zone. At sufficiently large negative phase values, the difference between the magnitudes of the pulse and trigger wave source currents increases with the magnitude of ξ. This reduces the pulse propagation speed by about 5% from the trigger wave value.

the slopes s_1, s_2, s_3, the coupling constant ζ, and the small parameter ε. For our present purposes, it suffices to fix s_1, s_2, s_3, and ζ and consider the variation of the propagation speed with u_* and ε. For a given value of ε, smaller values of u_* produce faster waves, while for fixed threshold u_*, faster waves are generated at smaller values of ε. Typical $c_0(u_*)$ and $c_0(\varepsilon)$ for excitable media are shown in Figs. 4(b) and 5(b), respectively. In both cases, the plane-wave speed decreases monotonically from a maximum value to a ''knee'' value, below which the wave is no longer stable (the knee is the point where $\partial c_0/\partial u_*$ or $\partial c_0/\partial\varepsilon$ becomes infinite). Rinzel and Keller [18] obtained similar dependences for a simple piecewise linear $i(u)$ and proved that the slow speed solutions below the knee were unstable. For a given u_* and small ε, the function $c_0(\varepsilon)$ for 1D solitary pulses or 2D plane waves can be approximated far from the knee as [19]

$$c_0(\varepsilon)=C_0-\chi\varepsilon, \tag{6}$$

where C_0 is the trigger wave ($\varepsilon=0$) speed and the constant χ depends on the threshold u_* (and all other temporarily fixed parameters). The method for computing the trigger wave speed C_0 is discussed in several recent papers [16,17,19–22]. Approximate analytical expressions for χ were reported in Refs. [4,23] for specific RDE systems.

In two dimensions, the local wave speed additionally depends on the front curvature κ. In the limit $\varepsilon=0$, the normal component C of the trigger wave velocity is approximately given by [23,24]

$$C=C_0+D\kappa, \tag{7}$$

where C_0 is the trigger plane-wave speed for a fixed u_*, D is the diffusion coefficient of u, and the curvature κ is defined to be negative for convex wave fronts. This expression is valid for small to moderate curvatures [15] and is derived under the condition that the wave front's spatial profile is quasistationary (i.e., it does not change appreciably over the front transition time scale L_0/C_0). The linear approximation (7) is often referred to as the ''eikonal'' relation for the medium [25,26]. Generally, $C(\kappa)$ is nonlinear at large curvatures and the critical curvature κ_{cr} corresponding to vanishing trigger wave speed can be rigorously defined by requiring that u and v be stationary, $\partial u/\partial t=0$, and $\partial v/\partial t=0$ [7]. When ε is nonzero, the dependence of the wave-front speed c on curvature is still linear for small κ, but the intercept c_0 and the slope $D'\equiv dc/d\kappa|_{\kappa=0}$ depend on ε. Using an elegant analysis, Zykov [27] derived an expression for $c(\kappa)$ for small κ and small ε, with the slope D' given by [12]

$$D'=D\left(1+\frac{\varepsilon\chi}{c_0}\right), \tag{8}$$

where χ is the same constant as in Eq. (7) and D is the diffusion coefficient of u. A more general expression for D' valid for all $\varepsilon<\varepsilon_{knee}$ (corresponding to stable propagation) was recently found by Pertsov, Wellner, and Jalife [28]:

$$D'=D\{1-(\varepsilon/c_0)(\partial c_0/\partial\varepsilon)\}, \tag{9}$$

where $c_0=c_0(\varepsilon)$ is the full dependence of the plane-wave speed on ε. Since the derivative $\partial c_0/\partial\varepsilon$ is negative and turns into negative infinity at $\varepsilon=\varepsilon_{knee}$, we see that the slope D' is a growing function of ε that diverges at $\varepsilon=\varepsilon_{knee}$.

At large curvatures, the function $c(\kappa)$ is nonlinear just as in the trigger wave case. However, the relation between c and κ expressed as $\kappa=\kappa(c)$ for convex fronts has an extremum at the point (κ_{c1},c_1). This point is presumed to represent the point of marginal stability separating the stable ($c>c_1$) and unstable ($c<c_1$) curved wave-front solution branches [29]. The quantity κ_{c1} is called the critical curvature for a continuous wave front (in contrast to a front with an exposed wave edge). It is important to note that propagation of a front with critical curvature κ_{c1} takes place with a nonvanishing critical speed c_1. As ε increases, $|\kappa_{c1}|$ decreases (the marginal stability point moves towards the speed axis) and must vanish when ε reaches ε_{knee} since this is the value at which plane waves ($\kappa=0$) become marginally

stable [29]. We note that this definition of the critical curvature assumes steady-state conditions and thus does not depend on the specific history of front evolution from which the configuration (κ_{c1},c_1) arose. These conditions exist when a steadily rotating spiral wave front is attached to the smallest possible impermeable, circular hole (when the hole radius is too small, the spiral front detaches due to its inability support curvature values larger that $|\kappa_{c1}|$) [29]. Generally, $c(\kappa)$ determined from the evolution of a small excited circular domain will depend on the initial conditions, such as the amplitude and duration of an externally applied stimulus, and the specific definition of the wave-front position. However, our analysis shows that as the wave front propagates further away from the source, the instantaneous speed and curvature values approach the history-independent $c(\kappa)$ asymptotically as κ goes to zero [11].

III. CELLULAR AUTOMATA MODEL WITH INHIBITION

In this section we generalize our recent CA model for simulating trigger waves [7] in two-dimensional, isotropic media to incorporate the effects of an inhibitory process on propagation. In the CA model, the medium is decomposed into squares with side Δx, whose positions on the lattice are randomized according to the Markus-Hess [30] scheme in order to smooth out the discreteness of the lattice. Each element is assigned two internal parameters, an excitation threshold K and an interaction circle radius R, and also two variables, a binary state variable U and an internal phase T, which tracks the time elapsed since the last excitation of the element. Each element is also assigned an internal parameter T_E, the exciting state duration, which is the amount of time an excited element contributes to the excitation of its neighbors (defined as elements located inside its interaction circle). The value of T_E for CA trigger waves must be infinity since these waves ''propagate'' infinitely long at zero speed. (In RDE models, the analogous property is the presence of nonzero excitatory source current over the u region delimited by $u_i<u\leqslant u_+$, which locally requires an infinite transition time to traverse). The state U of an element can assume two values, $U=0$ and $U=1$, which correspond to the resting and excited states, respectively. The CA transition rule states that the kth element switches from the resting state to the excited state at the next time step Δt when the ''total source'' Q_k contributed by its neighbors equals (or exceeds) its threshold value K_k (the ''sink''), that is, when

$$Q_k=\sum_{neighbors} w_{kj}U_j\geqslant K_k, \tag{10}$$

where the sum represents the total source (the summation index j runs over all elements in the neighborhood of element k), and w_{kj} is a weighting distribution determining the relative contribution of element j to the excitation of element $k(0\leqslant w_{kj}\leqslant 1)$. As in Ref. [7], we shall study the simplest case with $w_{kj}\equiv 1$ for all elements. For this realization of the model, the source Q_k for trigger waves is always equal to the number of excited elements inside the neighborhood circle.

The sum in Eq. (10) is an exact representation of an integral on a discrete lattice. This allows us to write the general CA transition rule for trigger waves in the compact form

$$U_{n+1}(\mathbf{x})=U_n(\mathbf{x})+[1-U_n(\mathbf{x})]\Theta\left(-K_{n+1}(\mathbf{x})+\int w(\mathbf{x}'-\mathbf{x})U_n(\mathbf{x}')d\mathbf{x}'\right), \tag{11}$$

where n is the discrete time index, $\Theta(\ )$ is the Heaviside step function, $w(\mathbf{x}'-\mathbf{x})$ is the weighting function describing the relative contribution of the neighbor at $\mathbf{x}'$ to the excitation of the element at $\mathbf{x}$, and $K_{n+1}(\mathbf{x})$ is the excitation threshold of the element at $\mathbf{x}$ at time step $n+1$. Note that our randomization of the lattice means that a complete simulation must incorporate an ensemble of systems that produce the expectation value of $U_{n+1}(\mathbf{x})$. Thus the complete form of Eq. (11) must incorporate the ensemble averaging of the right-hand side of Eq. (11) at each time step. For one particular realization of the lattice randomization, a trigger wave solution of Eq. (11) corresponds to a moving spatial discontinuity in the U field.

We simulate the effect of the ''recovery'' process on propagation by introducing a factor $S(S<1)$ under the integral in Eq. (11) to describe the decrease of an excited element's ''source intensity'' (its ability to excite its neighbors) with its phase T. This modification is suggested by our earlier analysis of the RDE trigger wave and solitary pulse source currents in the front transition zone. This revealed that the excitatory source current of the pulse reduces with time relative to that of the trigger wave, with $t=0$ set by the passage of a suitably defined wave-front edge. This effect is formally described in the CA model by introducing a phase-dependent, continuous-valued state variable $U=U(\mathbf{x},T)$, which without loss of generality can be factorized into the original binary variable $U=U(\mathbf{x})$, and a phase-dependent source intensity $S(\mathbf{x},T(\mathbf{x}))$ describing the local falloff of the source intensity. In a uniform medium, the source intensities S depend only on the local phase of the elements $T(\mathbf{x})$, so the expression for the total source $Q_n(\mathbf{x})$ becomes

$$Q_n(\mathbf{x})\equiv\int w(\mathbf{x}'-\mathbf{x})U(\mathbf{x}')S(T(\mathbf{x}'))d\mathbf{x}', \tag{12}$$

where the function S satisfies $S(0)=1$ and $S'(T)\leqslant 0$ for $T\geqslant 0$. For simplicity, we consider a simple one-parameter family of functions $S_\gamma=s(\gamma T)$, where $s(\ )$ is a fixed monotonically decreasing function of a dimensionless argument that specifies the model of recovery under consideration. The constant γ is a recovery rate with a dimension of inverse time. We explored several functions $s(\gamma T)$ and obtained very similar results.

Since we are currently only interested in the behavior of wave fronts, we choose the simplest representation of the wave back: The transition out of the excited state is a ''phase'' wave controlled solely by the local dynamics (phase T) at point $\mathbf{x}$. In this case, the transition to the resting state occurs at a particular phase $T=T_p(\mathbf{x})$, where $T_p(\mathbf{x})$ is the local duration of the pulse plateau. It follows that the exciting state duration $T_E(\mathbf{x})$ must satisfy $T_E(\mathbf{x})\leqslant T_p(\mathbf{x})$. The coupled equations describing the state transitions in the CA medium are thus

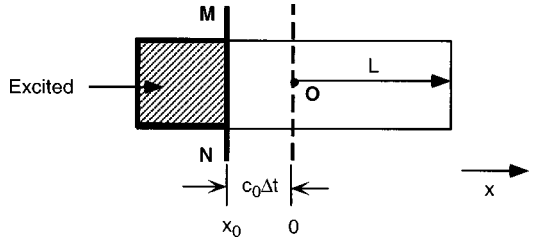

FIG. 3. Geometry for calculating the propagation speed c_0 of a 1D solitary front in the CA model (the underlying grid with spacing Δx is omitted). The neighborhood of point O is the segment $[-L,L]$, where L is the neighborhood ''radius.'' The wave front edge MN shifts to the point O at the next time step Δt when the total source strength Q provided by the excited elements (cross hatched) equals the excitation threshold K of the element at point O.

$$U'_{n+1}(\mathbf{x}) = U_n(\mathbf{x}) + [1 - U_n(\mathbf{x})]\Theta(Q_n(\mathbf{x}) - K_{n+1}(\mathbf{x})), \tag{13}$$

$$U_{n+1}(\mathbf{x}) = U'_{n+1}(\mathbf{x})\Theta(T_p(\mathbf{x}) - T(\mathbf{x})), \tag{14}$$

where $Q_n(\mathbf{x})$ is given by Eq. (12). A typical 1D U solitary pulse in a uniform medium traveling at speed c_0 will have a rectangular shape with unit height and width $c_0 T_p$ when viewed in a reference frame traveling with the wave.

IV. CA SOLITARY WAVE FRONTS IN ONE DIMENSION

The dynamical equations (13) and (14) can be treated analytically for the case of 1D solitary fronts. The notation is introduced in Fig. 3. The resting element at point O is chosen to be the element excited at the next time step Δt. The approaching wave of excited ($U=1$) elements is shown as the cross-hatched region. The element at point O switches to the excited state and the wave front MN shifts by the distance $c_0\Delta t$ when the argument of the Θ function in Eq. (13) becomes positive. This excitation condition is the marginal case where the total source $Q(\mathbf{x})$ exactly equals the threshold value $K(\mathbf{x})$ at point O:

$$K = Q \equiv \int w(\mathbf{x}')U(\mathbf{x}')S_\gamma(T(\mathbf{x}'))d\mathbf{x}'. \tag{15}$$

For a wave steadily propagating with speed c_0, the phase $T(x')$ at a point x' situated at a distance Δ behind the front is given by Δ/c_0. Since Δ can be written as $\Delta = |x' - x_0|$, where x_0 is the coordinate of the edge of the front, we have $T(x') = \Delta/c_0 = (x_0 - x')/c_0$. For a uniform medium with given w and S_γ, Eq. (15) establishes the relation between the threshold K, the recovery rate constant γ, and the propagation speed c_0.

We now seek the function $c_0(K,\gamma)$ for the simplest weighting function $w = \Theta(L^2 - x'^2)$ (a flat distribution over the interval $[-L,L]$ with unit height) and a linear dependence of the source intensity S on the phase T. We shall consider two cases: (i) a function $S(T) = 1 - \gamma T$ (and $T_E = \infty$), which may become negative, thereby severely inhibiting the wave-front transition for large γ or slow speed, and (ii) a piecewise linear function $S(T) = (1 - \gamma T)\Theta(1 - \gamma T)$, which vanishes for $T \geqslant 1/\gamma$ and thus satisfies the requirement $S \geqslant 0$. The second case is identical to setting $T_E = 1/\gamma$. We also assume that $T_p = \infty$ for all elements, so that there is no wave-back transition. For both cases of S, Eq. (12) for the total source Q becomes in dimensionless form

$$\hat{Q} = \int_{\hat{c}_0}^{x_m} \left\{ 1 + \hat{\gamma}\left(1 - \frac{\hat{x}}{\hat{c}_0} \right) \right\} d\hat{x}, \tag{16}$$

where $\hat{Q} = Q\Delta x/L$, $\hat{c}_0 = c_0\Delta t/L$, $\hat{x} = -x'/L$, $\hat{\gamma} = \gamma\Delta t$, and we have used the fact that $x_0 = -c_0\Delta t$. In case (i) the upper limit of the integral $x_m = 1$ and in case (ii) the upper limit is determined by the requirement $S \geqslant 0$, which yields

$$\hat{x}_m = \begin{cases} 1 & \text{if } \hat{c}_0 \geqslant \hat{\gamma}/(1+\hat{\gamma}) \\ \hat{c}_0(1+\hat{\gamma})/\hat{\gamma} & \text{otherwise.} \end{cases} \tag{17}$$

The dependence $c_0(K,\gamma)$ is found by calculating the integral in Eq. (16) and using the excitation condition (15) in the form $\hat{K} = \hat{Q}$, where $\hat{K} = K\Delta x/L$. In the case with the constraint $S \geqslant 0$ we find

$$\hat{K} = \begin{cases} 1 + \hat{\gamma} - \hat{c}_0 - \dfrac{\hat{\gamma}}{2}\left(\hat{c}_0 + \dfrac{1}{\hat{c}_0} \right) & \text{if } \hat{c}_0 \geqslant \hat{\gamma}/(1+\hat{\gamma}) \\ \dfrac{\hat{c}_0}{2\hat{\gamma}} & \text{otherwise.} \end{cases} \tag{18}$$

One can check that the two pieces on the right-hand side of Eq. (18) match smoothly at $\hat{c}_0 = \hat{\gamma}/(1+\hat{\gamma})$. For the case without the constraint, the expression in the first line of Eq. (18) determines the entire relation $c_0(K,\gamma)$ for all $\hat{c}_0 \geqslant \hat{\gamma}/(\hat{\gamma}+2)$.

The attractiveness of this simple one-dimensional example is that we readily see that for fixed $\hat{\gamma}$, the threshold and the speed are linked by a simple equation $f(\hat{K},\hat{c}_0) = 0$, where f is an explicit function depending on $\hat{\gamma}$ as a parameter. In case (i), when S is allowed to be negative, we obtain the family of hyperbolas shown in Fig. 4(a) (each curve is labeled by its $\hat{\gamma}$ value). In Fig. 4(b) we show the analogous plot obtained for a RDE model with kinetic functions similar to Eqs. (3)–(5) [31]. These curves are similar to those originally obtained by Rinzel and Keller [18], who proved that the slow speed solutions below the knee were unstable. It is broadly believed that this is true in the general case of a current $i(u)$ with three nodes [32]. In Appendix A we present a formal proof that the lower branch is also unstable in our CA model. The basic structure of the RDE and CA solutions is remarkably similar. This correspondence is also evident in the plot of $\hat{c}_0$ versus $\hat{\gamma}$ for fixed threshold values $\hat{K}$. This family of curves and the analogous family for the RDE model are shown in Figs. 5(a) and 5(b), respectively.

The intuitive appeal of our CA approach can be appreciated by a comparison of the dimensionless $c_0(K,\gamma)$ in Fig. 4(a) with that in Fig. 6, which is similar to Fig. 4(a), but obtained with the restriction $S > 0$ [case (ii)]. While each stable branch (including the knee point) remains unchanged, the behavior of the slow speed (unstable) branches in Fig. 6

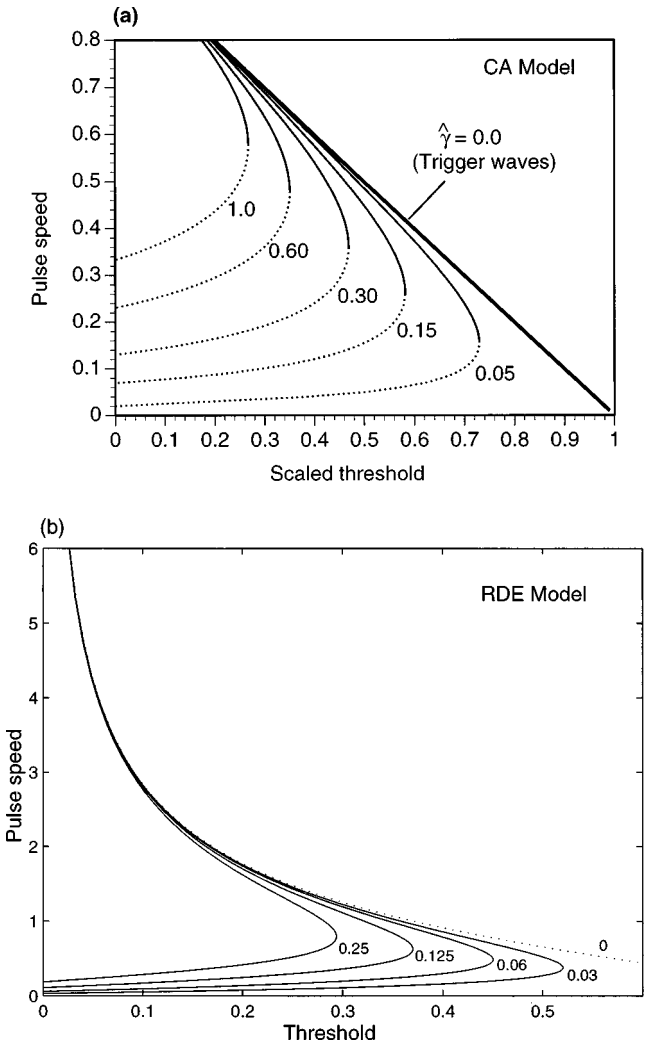

FIG. 4. (a) Dependence of the solitary front speed $\hat{c}_0$ on excitation threshold $\hat{K}$ for selected fixed recovery rate constants $\hat{\gamma}$ (labeled on each curve) in our CA model (a) [case (i), with no restriction on the sign of S] and (b) the analogous plot $c_0(u_*)$ for a RDE model similar to the system (3)–(5) [31]. In (b), the ε values are labeled on each curve. The slow-speed (dashed) solutions on the lower branches in (a) represent unstable CA wave-front configurations (see the proof in Appendix A). The instability of the slow-speed solution branch is broadly believed to be a general feature of continuous RDE systems [18,32].

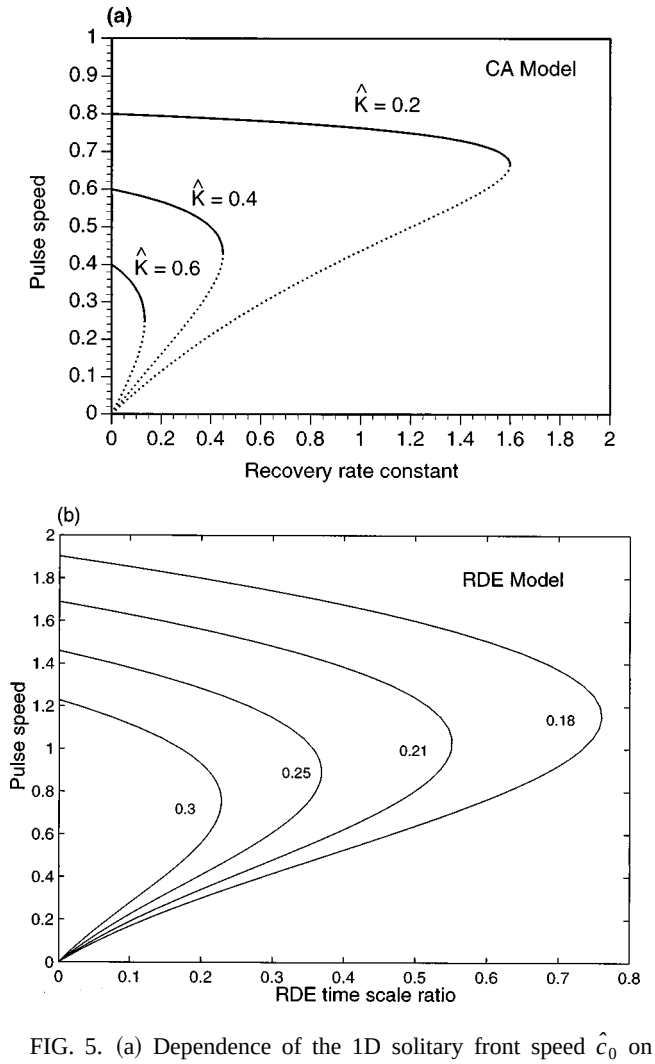

FIG. 5. (a) Dependence of the 1D solitary front speed $\hat{c}_0$ on recovery rate constant $\hat{\gamma}$ for selected fixed threshold values $\hat{K}$ (labeled on each curve) in our CA model [case (i), with no restriction on the sign of S] and (b) the analogous plot $c_0(\epsilon)$ for the same RDE model as in Fig. 4(b). In (b), the u_* values are labeled on each curve. The solutions on the lower branches are unstable.

is qualitatively different. To see the physical meaning of this discrepancy, we first point out that when the plot of the reaction source current in Fig. 2(b) for the RDE solitary pulse is extended to large negative ξ, we find that the wave-back transition is accompanied by large, positive (deexcitatory) currents. If we interpret the CA inhibitory process as a recovery process responsible for initiating a wave-back transition, then case (i) for S would be the appropriate physical model, as negative S could be associated with the wave-back transition. For the slowest-speed unstable solutions in Fig. 4(a), regions with negative S intrude in the CA interaction region. Due to the remarkable similarity of the RDE and CA slow-speed solution branches in Fig. 4, we infer that for the slowest-speed unstable RDE waves, the wave-back transition must interfere with the formation of the front. Such solutions must undoubtedly be unstable. Our CA model's simplicity allowed us to ascertain the physical source of this instability in the RDE system without resorting to more formal mathematical analysis.

V. CA PLANE-WAVE FRONTS

The geometry for computation of the plane-wave speed in two dimensions is shown in Fig. 7. The overlap of the domain of excited elements with the circle is outlined in bold. The wave front $MNPQ$ shifts to the point O at the next time step when the total source Q supplied by excited elements equals the threshold value K at point O in accordance with Eqs. (12) and (13). The new wave-front position shifted by the distance $c_0\Delta t$ after one time step is shown by the dashed line. We again assume a linear falloff of the local source intensity $S(T)$ and omit the restriction $S \geqslant 0$. The expression determining the total source Q is found by integrating $S(T(\mathbf{x}))$ with the weight $w(\rho)$ over the region outlined in bold in Fig. 7. Since we assume steady propagation, the local phase T of elements on the circular arc (hatched) is equal to $\Delta_0(\phi)/c_0$, where Δ_0 is the distance from the wave-front

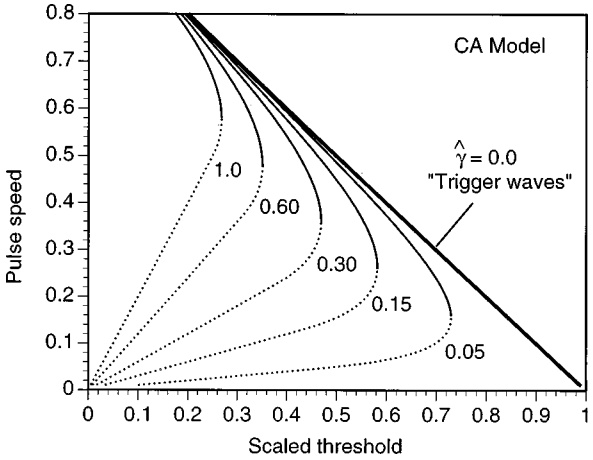

FIG. 6. Dependence of the solitary front speed $\hat{c}_0$ on excitation threshold $\hat{K}$ for selected fixed recovery rate constants $\hat{\gamma}$ (labeled on each curve) in our CA model with the restriction $S \geq 0$ [case (ii)]. The knee positions are identical to those in Fig. 4(a), but the slow speed branches are qualitatively different (see the text).

edge $MNPQ$. The local phase $T(\mathbf{x})$ is thus given by $[\rho\ \cos(\phi) - c_0 \Delta t]/c_0$. The excitation condition in dimensionless form can be written as

$$\hat{K} = \hat{Q} = 4 \int_{\hat{c}_0}^{1} w(\hat{\rho})\hat{\rho}\ d\hat{\rho} \int_0^{\omega(\hat{\rho};\hat{c}_0)} \left\{ 1 - \hat{\gamma} \frac{\hat{\rho}\ \cos\ \phi - \hat{c}_0}{\hat{c}_0} \right\} d\phi, \tag{19}$$

where $\hat{Q} = 2Q\Delta x^2/R^2$ and $\hat{K} = 2K\Delta x^2/R^2$ are the rescaled total source and threshold, respectively, and $\hat{c}_0 = c_0 \Delta t/R$, $\hat{\rho} = \rho/R$, and $\hat{\gamma} = \gamma \Delta t$. As can be seen in Fig. 7, the upper limit of the integral is $\omega(\hat{\rho};\hat{c}_0) = \arccos(\hat{c}_0/\hat{\rho})$.

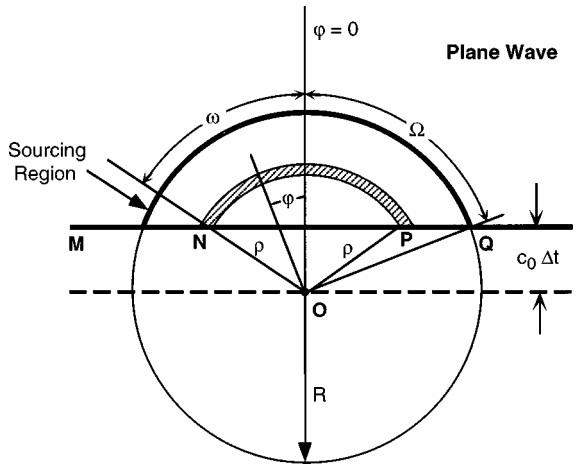

FIG. 7. Geometry for calculating the plane-wave speed c_0 in the 2D discrete model with circular support $(0 \leq \rho \leq R)$ of the weight function $w = w(\rho)$ (point O is the center of the neighborhood). The underlying grid is omitted. The wave front $MNPQ$ shifts to the point O at the next time step Δt when the total source strength Q provided by excited elements inside the region outlined in bold and given by Eq. (12) equals the excitation threshold K at point O. The new position of the wave front is shown as the dashed line. The angle definitions for integration are indicated.

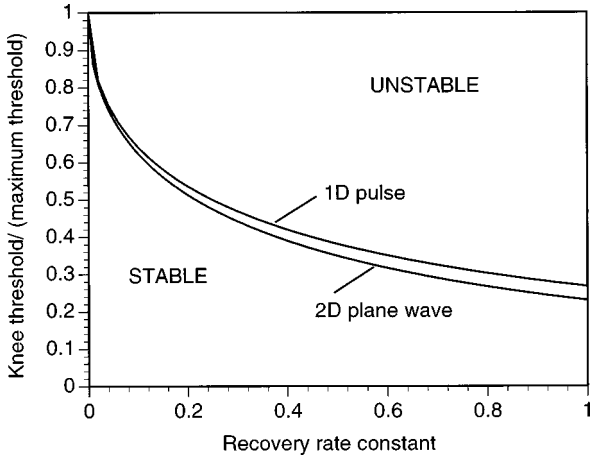

FIG. 8. Renormalized knee thresholds $\hat{K}/\hat{K}_{max}$ versus the recovery rate constant $\hat{\gamma}$ for 1D solitary front and 2D plane-wave fronts. These curves are neutral stability curves that divide the plane into stable and unstable front solution regions. The curves may also be interpreted as representing the maximum recovery rate constants $\hat{\gamma}_{max}$ as a function of the threshold $\hat{K}$. [Wave fronts with a given $\hat{K}$ can propagate only if $\hat{\gamma} \leq \hat{\gamma}_{\max}(\hat{K})$.]

Using the specific case $w(\hat{\rho}) = \Theta(1 - \hat{\rho})$, we interchange the order of integration and directly evaluate the integral

$$\hat{K} = 2\Omega(1 + \hat{\gamma}) - \frac{2\sqrt{1 - \hat{c}_0^{\,2}}}{\hat{c}_0} \left\{ \frac{2}{3}\hat{\gamma} + \hat{c}_0^{\,2} \left(1 + \frac{\hat{\gamma}}{3} \right) \right\}, \tag{20}$$

where $\Omega = \arccos\ \hat{c}_0$. This is an implicit equation determining the dependence $c_0(K, \gamma)$ for 2D plane-wave fronts.

For 2D plane-wave fronts, the family of curves $\hat{c}_0(\hat{K})$ for varying $\hat{\gamma}$ is similar to that obtained for the 1D case [Fig. 4(a)]. In the $(\hat{K},\ \hat{c}_0)$ plane, the knee coordinates trace out a neutral stability curve ($\hat{\gamma}$ is the parameter) that divides the plane into regions with stable and unstable wave-front solutions. For the 1D and 2D cases, we can find this parametrization explicitly by finding the extrema of the equation $\hat{K}(\hat{c}_0, \hat{\gamma})$, which gives

$$\hat{c}_{knee} = \sqrt{\hat{\gamma}/(\hat{\gamma} + d + 1)}, \tag{21}$$

where d is the dimension (1 or 2). The knee speeds increase monotonically with $\hat{\gamma}$ and approach unity asymptotically as $\hat{\gamma} \to \infty$. The monotonic growth of $\hat{c}_{knee}(\hat{\gamma})$ is physically sensible since for a fixed threshold an increase in the knee speed is needed to compensate for the increase in the recovery rate $\hat{\gamma}$ so that $Q = K$ is satisfied. This is because the decrement of source γT is proportional to γ/c_0. Expression (21) allows us to find the neutral stability curves in the $(\hat{\gamma}, \hat{K})$ plane by simply substituting into Eq. (18) (1D) and Eq. (20) (2D), respectively. These curves are plotted in Fig. 8. When $\hat{K}$ is treated as the independent variable, the curves in Fig. 8 can also be interpreted as representing the relation $\hat{\gamma} = \hat{\gamma}_{max}(\hat{K})$, which expresses the fact that for each $\hat{K}$, there is a maximum permissible recovery rate constant $\hat{\gamma} = \hat{\gamma}_{max}$ for a stable front.

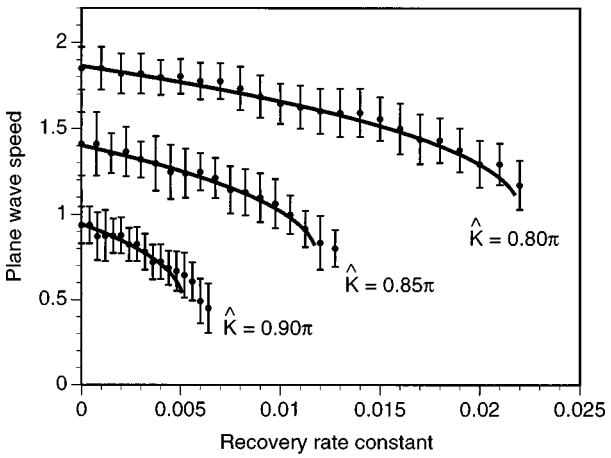

FIG. 9. Dimensionless plane-wave speed $c_0\Delta t/\Delta x$ versus recovery rate constant $\hat{\gamma}$ for selected (high) excitation thresholds $\hat{K}$ (low excitabilities). The curves are the theoretical values obtained using Eq. (20) and the dots are the averages obtained from simulations performed on a lattice with $R/\Delta x=12$ and with a correction for the discreteness of the phase $\hat{T}$ (see Appendix B). The error bars represent one standard deviation and reflect the fluctuations caused by the lattice randomization.

For the 1D case, these maxima correspond to the knee points of the curves shown in Fig. 5(a).

The stable branches of $\hat{c}(\hat{\gamma})$ for 2D plane waves given by Eq. (20) for selected fixed thresholds $\hat{K}$ are shown in Fig. 9 along with the results of CA simulations (dots). For small $\hat{\gamma}$, these curves may be approximated with the same precision as in the RDEs [Eq. (6)] by a function $\hat{c}_0(\hat{\gamma})=\hat{C}_0-\chi'\hat{\gamma}$, where $\hat{C}_0$ is the trigger wave speed and the constants χ' and $\hat{C}_0$ depend on the threshold $\hat{K}$. The simulations were performed on a 2D lattice with a periodic boundary condition in one direction (a cylinder). The CA elements were all assigned identical radii R and thresholds K. We computed the speed of the plane waves by tracking the position of the wave-front edge (averaged over random seed point locations) after each time step. The points in Fig. 9 are the average speeds and the error bars correspond to one standard deviation and reflect the intrinsic fluctuations induced by the randomization of the lattice. For the chosen threshold values (low excitabilities), the agreement between the theoretical curves and the CA simulations is excellent. The largest $\hat{\gamma}$ simulation value shown for each $\hat{K}$ was the maximum value for which the wave fronts were stable. There are two reasons for the deviations from the theoretical curves at large $\hat{\gamma}$ (near the knee). The first is due to the approximation of continuous phase used in Eq. (19) and the second is the specific method of assigning the actual element phases in the CA simulations, which we discuss in Appendix B.

VI. CA WAVE FRONTS WITH CURVATURE

In order to analyze the propagation of a curved CA solitary wave front, we evaluate the integral in Eq. (12) by approximating the front locally by a circle of radius r as shown in Fig. 10. For convenience, we define the dimensionless, rescaled curvature $\eta\equiv R\kappa\equiv\pm R/r$, with plus and minus corresponding to concave and convex, respectively. The domain of validity of the locality assumption (the approximation of the front as a circle) is $-\infty\leqslant\eta\leqslant 1$ and is discussed in detail in Ref. [7]. In the figure, the domain of contributing excited elements to the excitation of the element at point O is outlined in bold and the new wave-front position after one time step is shown by the dashed curve. The dimensionless physical parameters $\hat{c}$ and η are linked to the integration variables (ρ,ϕ) via the expression for the quantity $\nu=\pm|O'P|/R\equiv\pm r'/R$,

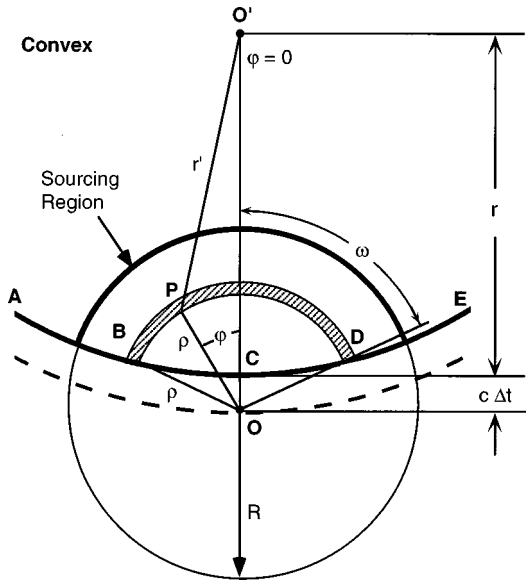

FIG. 10. Geometry for calculating the propagation speed c of a convex wave front in the CA model with a circular support ($0\leqslant\rho\leqslant R$) of the weight function $w=w(\rho)$ (point O is the center of the support region). The underlying grid is omitted. The wave front $ABCDE$ shifts to the point O at the next time step Δt when the total source strength Q provided by excited elements inside the region outlined in bold and given by Eq. (12) equals the excitation threshold K at point O. The new position of the wave front is shown as the dashed line. The wave front is locally approximated by a circle with radius r centered at the point O'. The angle definitions for the integration are indicated.

$$\nu^2=\hat{\rho}^2+\left(\hat{c}-\frac{1}{\eta}\right)^2-2\hat{\rho}\left(\hat{c}-\frac{1}{\eta}\right)\cos\,\phi, \tag{22}$$

where $\hat{\rho}\equiv\rho/R$ and we have adopted the same sign convention for ν as for η. The limits of the ϕ integration for each ρ are from $-\omega$ to $+\omega$, where ω is found by setting $\nu=1/\eta$ and $\phi=\omega$ in Eq. (22). This yields

$$\omega=\arccos\left\{\frac{\hat{\rho}^2-\dfrac{2\hat{c}}{\eta}+\hat{c}^2}{2\hat{\rho}\left(\hat{c}-\dfrac{1}{\eta}\right)}\right\}. \tag{23}$$

To assign a phase value T for each $(\hat{\rho},\phi)$ we will also require the expression for the distance $\Delta_\cap$ to the integration point from the wave-front edge $ABCDE$ directed along the inward normal, which in dimensionless form is given by $\hat{\Delta}_\cap=\nu-1/\eta$ (see Fig. 10). In the first approximation the

equation determining the phase T of a point at a distance $\hat{\Delta}_{\cap}$ from the front can be written as

$$\hat{T}=\frac{\nu-\dfrac{1}{\eta}}{\hat{c}}. \tag{24}$$

Generally, such a relation should incorporate the dependence on the specific history of evolution of the wave-front shape. Equation (24) is valid in the approximation where the front curvature κ is small and the speed c and curvature do not change appreciably in the neighborhood of point O (''steady propagation''). This approximation is identical to that used to obtain the eikonal relation (7) in RDE systems. Since the variable ν in expression (24) is a specific simple function $\nu(\hat{\rho},\phi;\hat{c},\eta)$ determined by Eq. (22), we have, according to Eq. (29), $\hat{T}=\hat{T}(\hat{\rho},\phi;\hat{c},\eta)$ and the excitation condition (13) applied to curved wave fronts becomes

$$\hat{K}=\hat{Q}\equiv 4\int_{\hat{c}}^{1} d\hat{\rho}\int_{0}^{\omega(\hat{\rho};\hat{c},\eta)}\{1-\hat{\gamma}\hat{T}(\hat{\rho},\phi;\hat{c},\eta)\}\hat{\rho}\; d\phi, \tag{25}$$

where the angle $\omega(\hat{\rho};\hat{c},\eta)$ is given by expression (23). Given the function $T(\hat{\rho},\phi;\hat{c},\eta)$, Eq. (25) explicitly expresses $\hat{K}$ as a function of $\hat{c}$, η and $\hat{\gamma}$. It also represents $\hat{c}$ as an implicit function of $\hat{K}$, $\hat{\gamma}$, and η. It is easy to check that in the limit $\eta\to 0$, Eq. (25) reduces to Eq. (19) and therefore yields the correct transition to the plane-wave limit. The solutions of Eq. (25) must generally be found numerically. In the following subsections, we consider the basic structure of these solutions and compare it to that found for typical RDE systems.

A. The critical curvature

In Sec. V, we identified the knee points of the family of curves $\hat{c}_0(\hat{K})$ for varying $\hat{\gamma}$ as the points of marginal stability of planar wave fronts. We now seek the dependence of these knee coordinates on the wave-front curvature η. For a fixed value of $\hat{\gamma}$, the solutions to Eq. (25) comprise a surface $F(\hat{c},\hat{K},\eta)=0$ as shown in Figs. 11(a) and 11(b). Since we are treating the curvature as a perturbation to the plane-wave case, we expect that for each fixed η contour [Fig. 11(b)], the lower solution branch represents unstable curved wave-front configurations. When the curvature effects are taken into account, the knee coordinates trace out a parametric curve in the $(\hat{K},\hat{c})$ plane with η as the parameter. If we intersect the surface F with a cutting plane $\hat{K}=\hat{K}_1=\text{const}$, with $\hat{K}_1$ less than the plane-wave ($\eta=0$) knee threshold value, we find that for each constant η contour we have two intersection points, a fast speed on the stable branch and a slow speed on the unstable branch. The locus of these points is the curve labeled $\hat{c}(\eta)$, which is the dependence of wave front speed on front curvature for $\hat{K}=\hat{K}_1$ and the specified $\hat{\gamma}$. When η reaches the critical value $\eta=\eta_{c1}$, the two intersection points merge with the knee point of $\hat{c}(\hat{K})$ as shown in Fig. 11(b). This defines for each $\hat{K}$ a critical point in the

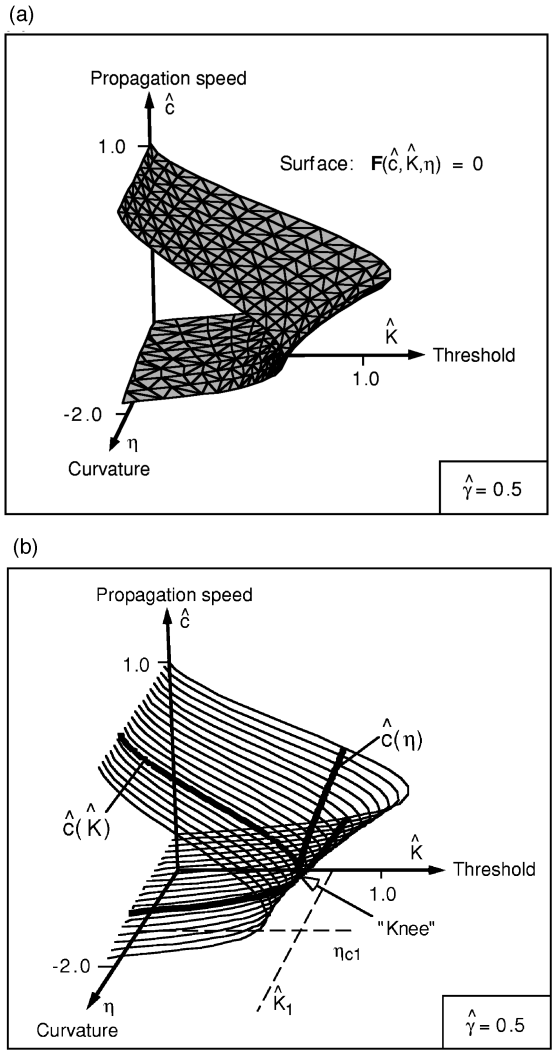

FIG. 11. Surface $F(\hat{c},\hat{K},\eta)=0$ (a) obtained from numerical solution of Eq. (25) for a fixed recovery rate constant ($\hat{\gamma}=0.5$) and (b) a set of its fixed η contours. At each fixed η, the lower branch of the contour (below the knee) represents unstable wave-front solutions. The curve labeled $\hat{c}(\eta)$ in (b) is the locus of points obtained by intersecting the surface F with the cutting plane $\hat{K}=\text{const}=\hat{K}_1$. This curve represents the dependence of the front speed $\hat{c}$ on the front curvature η for fixed $\hat{K}$ and $\hat{\gamma}$. Its lower branch is unstable. The η coordinate of the knee point of $\hat{c}(\eta)$ is the critical curvature η_{c1} (see text). Note also that the associated critical speed $c1$ is nonzero.

$(\eta,\hat{c})$ plane whose coordinate depends parametrically on the $\hat{\gamma}$ value used to specify the surface F. The η coordinate of this point we call the critical curvature η_{c1} and the $\hat{c}$ coordinate we call the critical speed $\hat{c}_1$. The critical curvature is (approximately) the maximum curvature at which a continuous convex wave front can stably propagate and is associated with a nonzero critical speed. This definition of the critical point is strictly valid in the stationary propagation approximation. When this approximation is not valid, the surface F is not unique and will depend on the specific history of evolution used to determine the phase function $T(\hat{\rho},\phi;\hat{c},\eta)$ in Eq. (25).

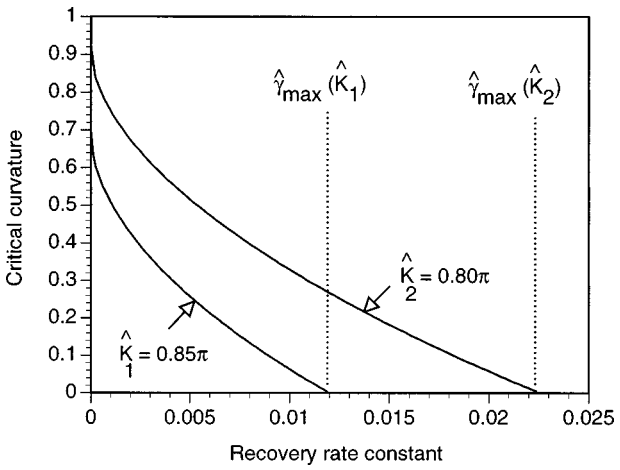

FIG. 12. Critical curvature η_{c1} versus recovery rate constant $\hat{\gamma}$ for two selected values of $\hat{K}$. The curves are very similar to that obtained for a RDE model by Mikhailov and Zykov (see Fig. 8 of Ref. [29]). For each threshold $\hat{K}$, the critical curvature must go to zero when $\hat{\gamma}$ reaches its knee value for plane waves $\hat{\gamma}_{max}(\hat{K})$ (see curves in Fig. 5).

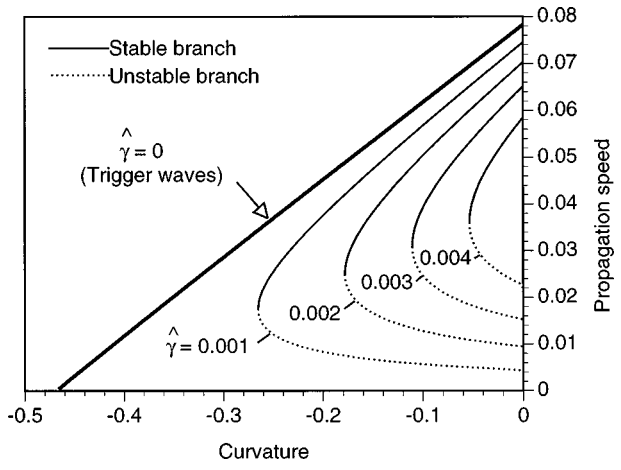

FIG. 13. Propagation speed $\hat{c}$ versus curvature $\hat{\eta}$ for fixed threshold $\hat{K} = 0.9\pi$ and selected values of the recovery rate constant $\hat{\gamma}$. The curve for trigger waves ($\hat{\gamma} = 0$) is shown in bold and is approximately linear due to the choice of a high excitation threshold. The slow speed (unstable) solutions are shown by the dashed portions of the curves. The dependence $\hat{c}(\eta)$ for each $\hat{\gamma}$ becomes strongly nonlinear near the critical curvature η_{c1}, where the derivative $d\hat{c}/d\eta$ becomes infinite. The plane-wave speed $\hat{c}_0$ (the intercept with the $\hat{c}$ axis) decreases with $\hat{\gamma}$. Note that the slope at $\eta = 0$ also depends on the recovery rate constant $\hat{\gamma}$. For the trigger wave case, we may identify this slope with the effective diffusion constant of the CA medium.

In their analysis of the relation $c(\kappa)$ in RDE systems, Mikhailov and Zykov [29] defined the critical curvature and speed for continuous wave fronts via the condition $dc/d\kappa = \infty$ for a fixed threshold u_*, fixed ε, and κ small. It is evident from Fig. 11(b) that in our CA model the condition $d\hat{c}/d\eta = \infty$ is satisfied at our critical point $(\hat{c}_1, \hat{K}_1, \eta_{c1})$, where the stable and unstable branches of $\hat{c}(\eta)$ meet. Thus our definition is equivalent to Mikhailov and Zykov's. Since the critical point in the CA model is also associated with the knee of $\hat{c}(\hat{K})$, we see that it is indeed a point of marginal stability. In Fig. 12 we plot the magnitude of the critical curvature versus $\hat{\gamma}$ for two selected values of $\hat{K}$. At the left edge $\hat{\gamma} = 0$ we get the trigger wave critical curvature, which is associated with a zero speed wave front. The critical curvature η_{c1} decreases to zero at a certain point $\hat{\gamma} = \hat{\gamma}_{max}(\hat{K})$. This is physically sensible since $\hat{\gamma}_{max}(\hat{K})$ is the knee value at which plane waves become marginally stable. The RDE neutral stability curve $\kappa_{c1}(\varepsilon)$ shown in Fig. 8 of Ref. [29] is very similar to our CA model $\eta_{c1}(\hat{\gamma})$.

B. The Eikonal relation

We now consider the variation of $\hat{c}(\eta)$ with $\hat{\gamma}$ and analyze its behavior at small curvatures η where the linear or eikonal approximation $\hat{c} = \hat{c}_0 + \hat{D}'\eta$ is applicable. The stable branch of the curve $\hat{c}(\eta)$ for fixed $\hat{K}$ and $\hat{\gamma}$ shown in Fig. 11(b) is monotonically decreasing with $\hat{c}(0) = \hat{c}_0$ and $\hat{c}(\eta_{c1}) = \hat{c}_1$. In Fig. 13 we show a family of curves $\hat{c}(\eta)$ for a fixed threshold $\hat{K}$ and selected values of $\hat{\gamma}$. We shall call such a curve a nonlinear curvature relation. The bold curve represents the trigger wave case ($\hat{\gamma} = 0$). The curves are fairly linear at small η and strongly nonlinear near the critical curvature, where the derivative $d\hat{c}/d\eta$ increases dramatically and becomes infinite at the critical point. The variations of the critical curvature, critical speed, and plane-wave speed with $\hat{\gamma}$ are clearly seen: As the recovery rate increases, the curve and its critical point are drawn toward the $\hat{c}$ axis and the plane-wave speed (the intercept with the $\hat{c}$ axis) decreases. At $\hat{\gamma} = \hat{\gamma}_{max}(\hat{K})$, the curve will collapse to a single point on the $\hat{c}$ axis (corresponding to zero critical curvature) since this is the point of marginal stability (knee) for plane waves. It is also evident from the figure that the derivative $\hat{D}' = d\hat{c}/d\eta$ at $\eta = 0$ is an increasing function of $\hat{\gamma}$ that will diverge as $\hat{\gamma}$ approaches $\hat{\gamma}_{max}(\hat{K})$. The $\hat{\gamma}$ dependence of our CA eikonal relation thus has the same characteristic features as the ε dependence of this relation in RDE systems [see Eq. (9)]. We computed the CA dependence of the slope $\hat{D}' \equiv (d\hat{c}/d\eta)|_{\eta=0}$ on $\hat{\gamma}$ numerically via Eq. (25) for selected fixed values of $\hat{K}$. The results are shown in Fig. 14. The slope $\hat{D}'$ increases monotonically with $\hat{\gamma}$ and indeed begins to diverge as $\hat{\gamma}$ approaches its maximum value (shown by the dashed lines in the figure). When $\hat{\gamma} = 0$, the slope is the trigger wave value and can be identified as the effective diffusion constant of the CA medium.

To examine the domain of validity of the steady propagation approximation and the numerically evaluated eikonal parameters D' and $\hat{c}_0$ for the CA medium, we performed simulations of evolving circular waves for various initial configurations. Excited circular regions of different sizes (with S initialized to 1.0) were created and the instantaneous wave-front speeds and front curvatures were calculated by measuring the average radial distance $\langle r_n \rangle$ to elements on the front (defined as excited elements with at least one adjacent resting neighbor) at time step n. The instantaneous speed

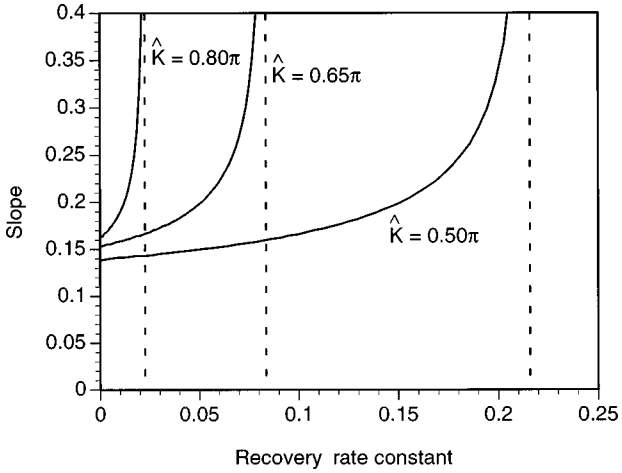

FIG. 14. Slope $\hat{D}=d\hat{c}/d\eta|_{\eta=0}$ versus recovery rate constant $\hat{\gamma}$ (solid lines) for selected fixed thresholds $\hat{K}$. The slope is a monotonically increasing function of $\hat{\gamma}$ that diverges as $\hat{\gamma}=\hat{\gamma}_{max}(\hat{K})$ (indicated by the vertical dashed lines). The maximum $\hat{\gamma}$ values correspond to the case of marginal stability of plane waves at the corresponding thresholds.

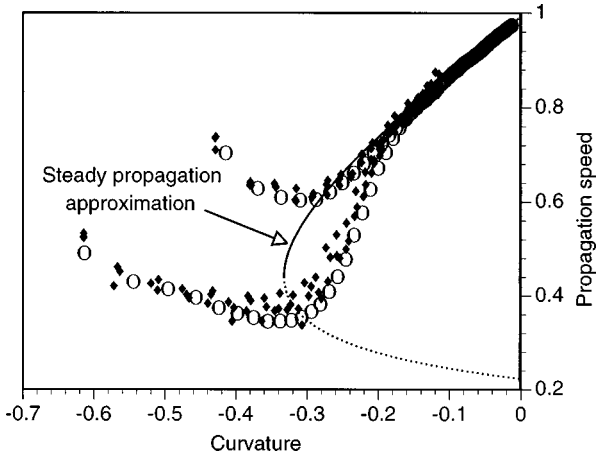

FIG. 15. Wave-front speed c versus front curvature κ in the CA model adjusted to a particular RDE system. The CA parameter values are listed in Fig. 16. The stable (solid line) and unstable (dashed line) branches of $c(\kappa)$ were obtained from numerical solution of Eq. (25), which assumes stationary (steady) propagation. The open circles O represent the instantaneous c and κ obtained from direct numerical solution of the evolution equations (13) and (14) for two specific stimulated ($S=1.0,\ \Delta t=1$) circular domains. The diamonds are the results of three different CA simulations (with different lattice randomizations) at each of the two initial conditions. The deviation from the steady propagation approximation at large curvatures is evident, as is the dependence on the specific initial condition. As the curvature magnitude decreases, the speeds and curvatures approach the stable branch of $c(\kappa)$ asymptotically.

measured in lattice units per time step was given by $\langle r_{n+1}\rangle - \langle r_n\rangle$ and the dimensionless curvature η was $-R_d/\langle r_n\rangle$, where R_d is the neighborhood radius measured in lattice units. The values of the CA parameters $R,\ K,\ \Delta t$, and γ were chosen by adjusting the CA model to the specific RDE system used in Sec. VII. The stable (solid) and unstable (dashed) branches of the CA model $c(\kappa)$ obtained via solution of Eq. (25) for these parameter values are shown in Fig. 15. The circles in the figure represent the theoretical evolution of two different sized circular excited regions computed directly via numerical solution of equations (13) and (14) with $T_p=\infty$. The solid diamonds show the results of three different simulations (each with a different lattice randomization) at each initial configuration in the CA model. The fluctuations induced by the lattice randomization are evident, but the agreement with theoretical predictions is very good. We see that for small to moderate curvatures, a linear eikonal relation $c=c_0+D'\kappa$ adequately represents the behavior of the CA wave fronts in all three approaches represented in the figure.

Two important features of excitable media can be illustrated using Fig. 15. First, notice that at large curvatures near the critical value κ_{c1}, the actual speed-curvature dependence is sensitive to the initial conditions, but as the magnitude of the front curvature decreases, the points converge to the nonlinear curvature relation $c(\kappa)$ obtained assuming steady propagation. This dependence on the history of evolution means that a unique critical curvature may not exist in excitable media. The critical value κ_{c1} defined above is approximately realized only for the special history-independent case of a spiral wave front steadily rotating around a minimally sized, impenetrable hole. This was successfully demonstrated for a RDE system in Ref. [29]. The second important feature is that the inhibitory process affects the specific size-strength-duration relation for applied stimuli that can successfully generate propagating waves [33–35]. For the two cases shown in Fig. 15, the duration of the stimulus was one time step and for an initial S value of 1.0 we found that a minimum circle radius (with a maximum curvature) was required to generate an outgoing wave (for smaller radii the wave died out). The ''threshold'' radius case is represented by the lower set of points in the figure. When we applied the stimulus for a longer duration (not shown) with S maintained at 1.0 for multiple time steps, smaller excited circles (with larger curvatures than the threshold value) successfully produced propagating waves. Physically, this is due to the retardation of local recovery effects in the stimulated region via ''currents'' supplied by the stimulating device itself. We plan a thorough analysis of this phenomenon in a future study.

VII. CA SPIRAL WAVE FRONTS

As a final illustration of the correspondence between our CA model and RDE models of the form (1) and (2), we consider a steadily rotating spiral wave in the CA model adjusted to a particular RDE system. In contrast to the simulations depicted in Fig. 15, where the front speeds and front curvatures vary with time, a steadily rotating spiral is a steady-state configuration (in a rotating reference frame) in which the front curvature and speed (in the normal direction) vary according to a specific function of arclength along the spiral arm. (The stationarity of the spiral in the rotating frame may just be a first approximation. In reality, the influence of the exponentially decaying tail of the wave may introduce a small but ever-present, nonvanishing perturbation.) Since we are currently considering wave fronts that do not interact with wave tails, we are restricted to a specific class of spiral waves for our analysis. The dynamics of spiral

waves is controlled by the medium's excitability, the rate of recovery of excitability following the wave-back transition, and the boundary conditions. If the extent of the medium is sufficiently large and the excitability is sufficiently weak, spiral waves rotate around a quiescent (unexcited) circular core at a unique characteristic frequency of the medium. In the ''thin arm'' regime [15], the interaction of the wave front with its previous wave tail is negligible and the front speed c is determined almost entirely by the nonlinear curvature relation $c(\kappa)$ (provided the front curvature radius near the spiral tip is much larger than the wave-front thickness [3,15]). In this domain, the motion of most of the spiral (away from the tip) is well described via a kinematic model [27,36], in which the wave is treated as a curve in the plane that obeys certain equations of motion that depend on $c(\kappa)$. The kinematic analysis of spirals in RDE systems has proved successful in describing the results of numerical solutions [29]. Here we check the predictions of kinematic theory in our CA model by directly comparing the CA and RDE spiral solutions for the CA model adjusted to a specific RDE system.

We use a RDE system with kinetic functions (3) and (4) and the current $i(u)$ given by

$$i(u)=\begin{cases} s_1 u & \text{when } u \leqslant u_* \\ s_2(u-1) & \text{when } u > u_* . \end{cases} \tag{26}$$

Based on trial solutions and recent studies of this system [4], we found that the parameter values $s_1=1.0$, $s_2=1.0$, $\zeta=7$, $\varepsilon=0.02$, and $u_*=0.25$ yielded a spiral wave satisfying the thin arm requirement. The trigger wave speed C_0 and the trigger wave critical curvature κ_{cr} were calculated for these parameter values using the expressions in Refs. [7,17]. We obtained $C_0=1.15$ and $\kappa_{cr}=0.94$ (in the chosen units $D=1.0$). The plane solitary wave speed $c_0(\varepsilon)$ was measured via numerical solutions using explicit Euler integration for the recovery equation (2) and a forward time-centered finite-difference scheme [37] for the diffusive equation (1). For the discretizations $h=0.2$ (grid spacing) and $\delta t=0.002$ (time step), the measured plane-wave speed was $c_0=1.0$. The duration of the plateau phase for the plane wave was 6.95 (defined as the time interval between the crossings at $u=u_*$) and T_p and T_E were set equal to this value in the CA model. The medium was considered fully recovered when v returned to 0.02, which occurred at $T=26.65$.

The procedure for computing the CA parameter values for the medium in the trigger wave limit is described in Ref. [7] and uniquely determines the values of the circle radius R, the scaled threshold $\hat{K}$, the time step Δt for given RDE solution values of C_0 and κ_{cr}, and the RDE diffusion constant D. The remaining CA model parameter value $\hat{\gamma}$ is found by equating the plane-solitary-wave speed c_0 to the quantity $\hat{c}_0 R/\Delta t$, with C_0 obtained from Eq. (20). To simulate an infinite medium, we also had to use no-flux boundary conditions along the edges of the grid. These conditions were only implemented approximately [38], but the measured CA spiral period and shape (see below) did not change noticeably when the domain size was increased by 25%. Our approximation was thus sufficient for our present purposes.

We created the spiral waves via a broken plane-wave initial condition. The numerical solution of the RDEs and the CA spiral wave are shown in Fig. 16. In both pictures, the grid spacing Δx is approximately 0.2 and the grid size is 250×250. White regions represent resting elements ($v<0.02$ in the RDEs), black represents excited elements ($u>u_*$ in the RDEs), and gray regions represent unexcited (recovering) elements. The rotation periods are 73.3 and 71.3 in the CA and PDE models, respectively. Note that the spiral shapes are practically identical along the spiral arm except in the vicinity of the core. In this region, the specific value of T_E and also the details of the wave back transition are important in determining the CA spiral tip shape and the rotation period. The almost exact correspondence of the CA and RDE periods was thus fortuitous. According to the kinematic theory of spirals, for a spiral with a given rotation period, the shape away from the tip is unique and depends only on $c(\kappa)$ [29]. The remarkable similarity of the CA and RDE spirals suggests that this dependence must be roughly the same in both systems. We computed the slope D' of the eikonal relation for the RDE system using expressions (6) and (9) and found $D'\approx1.14$, which is in good agreement with the $\hat{\gamma}$-dependent CA model value of 1.19. Good correspondence was also obtained when the grid spacing in both models was reduced by 50% (the stability of the solution method also required the reduction of the RDE model time step). The consistency of the CA spiral shape with that predicted by the kinematic theory of spiral waves for our $c(\kappa)$ was studied in detail in Ref. [39] and excellent agreement was found.

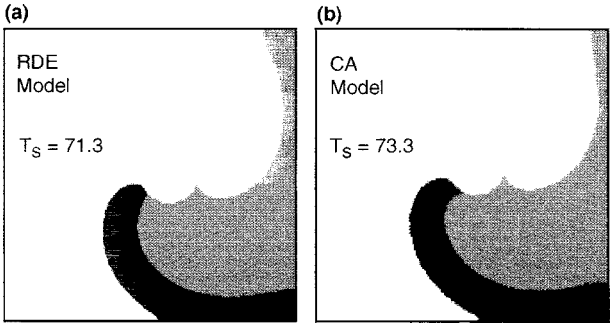

FIG. 16. (a) Spiral waves in the RDE model (1) and (2) with kinetic functions (3) and (4) and $i(u)$ given by Eq. (26) and (b) the CA model adjusted to the RDEs. The RDE model parameter values were $s_1=1.0$, $s_2=1.0$, $u_*=0.25$, $\zeta=7.0$, and $\varepsilon=0.02$. The CA parameter values obtained using our adjustment criteria were $R=1.65$, $\Delta t=0.42$, $\hat{K}=2.025$, and $\hat{\gamma}=0.044$. The black regions are excited elements ($u\geqslant u_*$ in the RDEs), gray regions are recovering, and white regions are resting. The rotation periods are approximately the same: (a) $T_{spiral}=71.3$ and (b) $T_{spiral}=73.3$. The correspondence between the spiral shapes is excellent, except near the spiral core. Since the ''eikonal'' relations $c(\kappa)$ in both systems are approximately the same, kinematic theory demands that the shapes along the arms agree since the shape is uniquely determined by $c(\kappa)$ for a given rotation frequency in a sufficiently large medium [29].

ACKNOWLEDGMENTS

This work was supported by NASA Grant No. NAGW-4989, a grant from the National Space Biomedical Research Institute, and a grant from the Nihon Kohden Corporation. A. B. F. is grateful for financial support provided by the

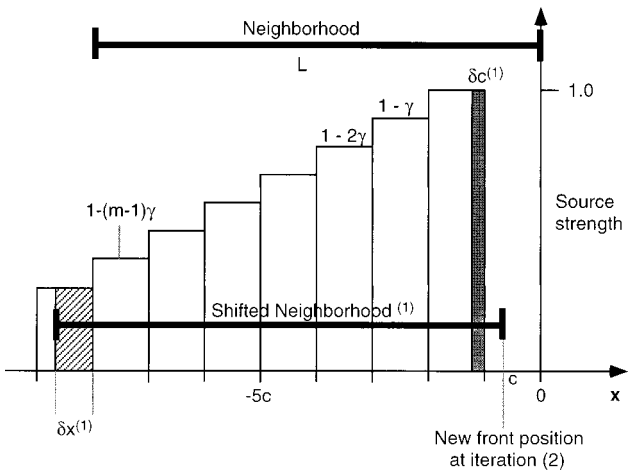

FIG. 17. Perturbation of the 1D CA wave front. The neighborhood radius L is indicated by the solid horizontal bars. The source strength of each element in the transition region L depends on its phase T and the recovery rate constant γ: $S(T)=1-\gamma T$. For a steadily propagating wave, the spacing between zones of equal S values is given by the propagation speed c. The initial perturbation of the front edge by the amount $\delta c^{(1)}$ requires a shift in the neighborhood by a distance $\delta x^{(1)}$ in order for the integral Q of the sources inside the transition zone to remain equal to the excitation threshold K. This shift results in a perturbation of the front speed $\delta c^{(2)}$ at the next time step and so on. After m steps, the spacing between the equal S value zones is no longer uniform, but the sum of these spacings can be used to estimate the magnitude of the final speed perturbation δc.

North American Society of Pacing and Electrophysiology.

APPENDIX A: INSTABILITY OF THE LOWER BRANCH OF $c=c(K)$

We consider a 1D solitary wave that propagates steadily along the x axis and define its propagation speed c to be the dimensionless distance that the wave front shifts in one time step Δt. For 1D solitary pulses and 2D plane waves, the CA time step can be chosen freely [7] and for convenience we choose it in such a way that the radius L of the neighborhood $[-L,L]$ is an integer multiple of c:

$$c(m+1)=L, \tag{A1}$$

where m is an integer and $L=1$ in our chosen units. For a steadily propagating wave, the local source intensity $S(T(x))$ is a stepwise function (a staircase with equal step widths) as shown in Fig. 17. We now slightly perturb the position of the front so that the width of the first step becomes $c^{(1)}=c+\delta c^{(1)}$. We consider a negative perturbation $\delta c^{(1)}<0$, which we believe must be the most dangerous, as such a perturbation leaves a solution on the lower branch of $c=c(K)$ on the lower branch. At the instant we perturb the front position, the source contribution from steps $2,3,\ldots,m$ on the staircase does not change, while the source contribution of the front step decreases by $|\delta c^{(1)}|$. Now, in order to satisfy the excitation condition $Q=K$ (conservation of sourcing) this decrease must somehow be compensated. This can come only from the rear of the sourcing zone (near the neighborhood boundary) which is forced to overlap a portion of step $m+1$, which has a source intensity $1-\gamma m$. [Recall that in our model the source intensity S is $1-\gamma T(x)$, thus the source intensity of the jth step is $S_j=1-\gamma(j-1)$.] The rear boundary of the transition zone must shift backward due to the perturbation by some $\delta x^{(1)}(\delta x^{(1)}<0)$, which can be found from the condition of conservation of sourcing $(1-\gamma m)\,\delta x^{(1)}=\delta c^{(1)}$. Since L is fixed, this gives rise to a perturbation in the position of the front at the next time step, so that two sourcing steps now possess perturbed widths. At the next time step, the third step width is perturbed and so on until the width of the mth step is perturbed. (One can show by direct calculations that the signs of all the respective perturbations are the same as that of $\delta c^{(1)}$: all steps become shorter, which is true for any source that decreases with time.) The backward shift of the rear boundary of the neighborhood $\delta x^{(m)}$ arising after m time steps is related to the radius of the neighborhood, the widths $c+\delta c^{(i)}$ of the first m steps $(i=1,2,\ldots,m)$, and the final perturbation of the speed δc by the condition that their widths sum up to the neighborhood radius

$$-\delta x^{(m)}+mc+\sum_{i=1}^{m}\delta c^{(i)}+c+\delta c=L. \tag{A2}$$

Using Eq. (A1) we reduce Eq. (A2) to

$$\delta c=\delta x^{(m)}-\sum_{i=1}^{m}\delta c^{(i)}. \tag{A3}$$

Now the conservation of sourcing can be written as

$$(1-\gamma m)\,\delta x^{(m)}=\sum_{i=1}^{m}[1-\gamma(i-1)]\,\delta c^{(i)}. \tag{A4}$$

Eliminating $\delta x^{(m)}$ from Eqs. (A3) and (A4) we have

$$\delta c=\sum_{i=1}^{m}\frac{\gamma(m+1-i)}{1-\gamma m}\,\delta c^{(i)}=\frac{\gamma}{1-\gamma m}\sum_{j=1}^{m}j\,\delta c^{(m+1-j)}. \tag{A5}$$

Using the fact that all $\delta c^{(k)}$ have the same sign, we can now estimate the perturbation δc as

$$|\delta c|=\frac{\gamma}{1-\gamma m}\sum_{j=1}^{m}j|\delta c^{(m+1-j)}|\geqslant\frac{\gamma|\delta c^{(j)}|_{min}}{1-\gamma m}\sum_{j=1}^{m}j. \tag{A6}$$

This finally yields

$$|\delta c|>\frac{\gamma m^2}{2(1-\gamma m)}|\delta c^{(j)}|_{min}\equiv q|\delta c^{(j)}|_{min}. \tag{A7}$$

If the factor q is greater than unity

$$q=\frac{\gamma m^2}{2(1-\gamma m)}>1, \tag{A8}$$

then after each m steps the minimum perturbation acquires the factor q and therefore grows as a geometric progression with the common ratio $q^{1/m}>1$. Now in the 1D case under consideration, one can readily prove that the condition (A8)

is equivalent to the requirement that the speed c belongs to the lower branch of the curve $K=K(c)$. Indeed, one can determine the marginal value of the speed that separates the upper and lower branches by taking a derivative of Eq. (18) and setting it to zero, which according to Eq. (21) yields

$$\frac{1}{c_{0,min}}=\sqrt{1+\frac{2}{\gamma}}, \tag{A9}$$

and using Eq. (A1) we finally obtain

$$m_{max}=-1+\sqrt{1+\frac{2}{\gamma}}. \tag{A10}$$

Now one can readily check that the condition $m<m_{max}$ is equivalent to the condition (A8), which completes our proof. The above analysis reveals the remarkable fact that the exponential growth of the perturbations does not occur with each time step but rather takes place after each time the wave shifts the distance L. This confirms our previous identification of the neighborhood radius as the intrinsic physical width of the excitation wave front [7].

APPENDIX B: CORRECTION FOR DISCRETE TIME IN THE CA MODEL

While the lattice randomization in the CA model provides the correction for the discreteness of space (i.e., it guarantees rotational and translation invariance on the average), the basic CA model provides no similar averaging in the time domain. This limitation cannot be overcome by simply further reducing the time step value, since in our simple four-parameter model for nonplanar wave fronts, this quantity is fixed by the requirements of the correct trigger wave limit [7]. In discrete time, a newly excited CA element is assigned a dimensionless phase $\hat{T}=T/\Delta t=0$. In this case, the contribution of these elements to the integral in Eq. (19) is simply $\Delta\hat{x}^2$, where $\Delta\hat{x}$ is the element size in units of R. This magnitude clearly exceeds the contribution $(1-\hat{\gamma}\Delta\hat{x}/\hat{c}_0)\Delta\hat{x}^2$ obtained when time is approximated as being continuous. More importantly, when the front shift in one time steps exceeds half of the interaction radius R (low thresholds), the model does not ''feel'' the recovery effects at all since all elements in the interaction circle will have phases $\hat{T}=0$. To correct for this discretization artifact in the simulations, each element's source intensity is computed via the expression $S=1-\hat{\gamma}(\hat{T}+\frac{1}{2})$. For the high thresholds ($\hat{K}$ near π) shown in Fig. 9, this adequately adjusts the model behavior to correspond to the theoretical values obtained by treating time as continuous (though the knee points do not exactly coincide). On the other hand, for low thresholds ($\hat{K}<\pi/2$), the CA realization of the continuous time behavior is not as good quantitatively (but the dependence of the speed on γ is still physically sensible). In Fig. 18 the bold curves are the solutions of Eq. (19), while the dotted curves correspond to the special case where the integrand is not dependent on the phase, but given by the constant $S=1-\hat{\gamma}/2$. The exact correspondence of the simulation points with the dotted curve for the smallest threshold is because in this case the phase $\hat{T}$ of every element inside the circle is zero. Thus, even at high excitabilities the CA model gives physically reasonable behavior and is predictive. For most cases of interest [7], the threshold values $\hat{K}$ required to adjust to specific RDE systems exceed $\pi/2$ and the solutions of Eq. (19) adequately describe the behavior of the CA model.

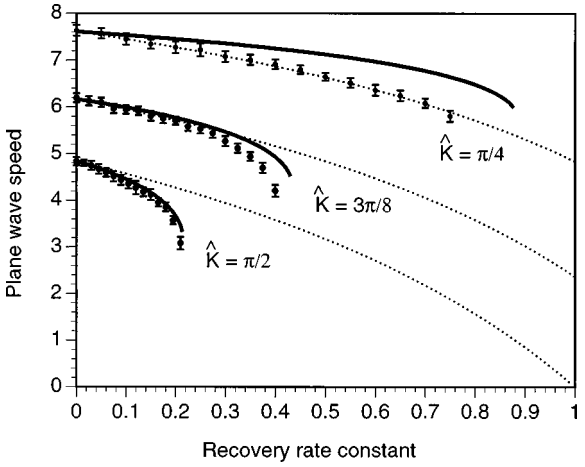

FIG. 18. Same as Fig. 9, but for low excitation thresholds $\hat{K}$ (high excitabilities). The bold curves are the stable branches of $\hat{c}=\hat{c}(\hat{\gamma})$ according to Eq. (20) and the dotted curves correspond to the solutions of Eq. (19) for the special choice of S as a constant, $S=1-\hat{\gamma}/2$. At the lowest threshold value shown, all contributing excited elements in the neighborhood of a given element have a dimensionless phase coordinate $\hat{T}=0$ and thus the model cannot ''feel'' the source falloff due to recovery. In such cases, the plane-wave speeds are given by the dotted curves.

[1] D. Mollison, J. R. Stat. Soc. **39**, 283 (1977).
[2] C. Luo and Y. Rudy, Circ. Res. **74**, 1071 (1994).
[3] J. M. Starobin and C. F. Starmer, Phys. Rev. E **54**, 430 (1996).
[4] J. M. Starobin, Y. I. Zilbeter, E. M. Rusnak, and C. F. Starmer, Biophys. J. **70**, 581 (1996).
[5] J. M. Starobin and C. F. Starmer, Phys. Rev. E **55**, 1193 (1997).
[6] J. M. Starobin, C. F. Starmer, and A. J. Starobin, Phys. Rev. E **56**, 3757 (1997).
[7] Y. B. Chernyak, A. B. Feldman, and R. J. Cohen, Phys. Rev. E **55**, 3215 (1997).
[8] M. Gerhardt, H. Schuster, and J. J. Tyson, Physica D **46**, 416 (1990).
[9] V. G. Fast and I. G. Efimov, Physica D **49**, 75 (1991).
[10] J. R. Weimar and J. Boon, Phys. Rev. E **49**, 1749 (1994).
[11] A. B. Feldman, Y. B. Chernyak, and R. J. Cohen (unpublished).
[12] A. T. Winfree, Int. J. Bifurcation Chaos **7**, 487 (1997).

[13] A. M. Pertsov, E. A. Ermakova, and A. V. Panfilov, Physica D **14**, 117 (1984).
[14] J. J. Tyson and J. P. Keener, Physica D **29**, 215 (1987).
[15] E. Meron, Phys. Rep. **218**, 1 (1992).
[16] Y. B. Chernyak, in *Proceedings of the 18th Annual International Conference of the IEEE Engineering in Medicine and Biology Society*, edited by H. Boom *et al.* (IEEE, New York, 1996), paper 931.
[17] Y. B. Chernyak, Phys. Rev. E **56**, 2061 (1997).
[18] J. Rinzel and J. B. Keller, Biophys. J. **13**, 1313 (1973).
[19] A. S. Mikhailov, *Foundation of Synergetics I. Distributed Active Systems* (Springer-Verlag, New York, 1990).
[20] A. B. Feldman, Y. B. Chernyak, and R. J. Cohen, in *1995 IEEE Engineering in Medicine and Biology 17th Annual Conference, and 21st Canadian Medical and Biological Engineering Conference* (IEEE, New York, 1995), p. 21.
[21] J. Starobin, Y. I. Zilbeter, and C. F. Starmer, Physica D **70**, 321 (1993).
[22] R. D. Benguria and M. C. Depassier, Phys. Rev. Lett. **77**, 1171 (1996).
[23] V. S. Zykov, Biofizika **25**, 888 (1980) [Biophysics (Engl. Transl.) **25**, 906 (1980)].
[24] J. P. Keener, SIAM (Soc. Ind. Appl. Math.) J. Appl. Math. **46**, 1039 (1986).
[25] P. C. Franzone and L. Guerri, Math. Biosci. **101**, 155 (1990).
[26] P. K. Brazhnik and J. J. Tyson, Phys. Rev. E **54**, 4338 (1996).
[27] V. S. Zykov, *Simulation of Wave Processes in Excitable Media* (Nauka, Moscow, 1988) [translated by A. T. Winfree (Manchester University Press, Manchester, 1988)].
[28] A. M. Pertsov, M. Wellner, and J. Jalife, Phys. Rev. Lett. **78**, 2656 (1997).
[29] A. S. Mikhailov and V. S. Zykov, Physica D **52**, 379 (1991).
[30] M. Markus and B. Hess, Nature (London) **347**, 56 (1990).
[31] Y. B. Chernyak, J. S. Starobin, and R. J. Cohen, Phys. Rev. Lett. (to be published).
[32] P. Fife, J. Chem. Phys. **64**, 554 (1976).
[33] B. N. Belintsev, B. F. Dibrov, M. A. Livshits, and M. V. Volkenstein, Biofizika **23**, 864 (1978).
[34] J. Starobin, Y. I. Zilbeter, and C. F. Starmer, Physica D **70**, 321 (1994).
[35] J. C. Neu, R. S. Preissig, Jr., and W. Krassowska, Physica D **102**, 285 (1997).
[36] A. S. Mikhailov, V. A. Davydov, and V. S. Zykov, Physica D **70**, 1 (1994).
[37] D. Barkley, M. Kness, and L. Tuckerman, Phys. Rev. A **42**, 2489 (1990).
[38] A. B. Feldman, Ph.D. thesis, Harvard University 1996 (unpublished).
[39] A. B. Feldman, Y. B. Chernyak, and R. J. Cohen, in *Proceedings of the 19th Annual International Conference of the IEEE Engineering in Medicine and Biology Society*, edited by R. Jaeger and G. Agarwal (IEEE, New York, 1997), paper 413.